Calculated out-of-plane transmission loss for photonic-crystal slab waveguides

Wan Kuang, Cheolwoo Kim, Andrew Stapleton, Woo Jun Kim, and John D. O'Brien

Department of Electrical Engineering-Electrophysics, University of Southern California, Powell Hall of Engineering, 3737 Watt Way, Los Angeles, California 90089-0271

Received May 13, 2003

A fully three-dimensional finite-difference time domain numerical model is presented for calculating the out-of-plane radiation loss in photonic-crystal slab waveguides. The propagation loss of a single-line defect waveguide in triangular-lattice photonic crystals is calculated for suspended-membrane, oxidized-lower-cladding, and deeply etched structures. The results show that low-loss waveguides are achievable for sufficiently suspended membranes and oxidized-lower-cladding structures.

OCIS code: 230.7370.

Two-dimensional photonic-crystal defect waveguides have been the subject of active research recently because of their potential to be a basic building block for densely integrated optics. They are most simply formed by inserting a linear defect into a two-dimensional triangular lattice of air holes in a dielectric slab. All the proposed and demonstrated photonic-crystal waveguides, however, are not rigorously guided and suffer from radiation loss. We utilize a fully three-dimensional (3-D) finite-difference time domain (FDTD) model to predict the out-of-plane losses.

Holes with radii of $r/a = 0.3$ arrayed in a triangular lattice are made to perforate five dielectric structures, which are detailed in Table 1. Of these five structures two are suspended-membrane structures that differ in their suspension distance above a GaAs substrate. Distances of normalized thickness $d/a = 1.0$ and $d/a = 3.0$ are considered here. Two other waveguide geometries in which the membranes have asymmetric air–top and oxide–bottom cladding layers are considered with oxide thicknesses d/a of 2.0 and 5.0. Finally, a deeply etched structure in which the photonic crystal extends through the $Al_xGa_{1-x}As$ lower-cladding layer is included. All five structures have a GaAs substrate. We limit our study to defect waveguides formed by removing a single row of holes along the $\Gamma - K$ direction, as shown in Fig. 1.

The structures are modeled with a 3-D FDTD method with a message-passing interface to run in a parallel environment.[1,2] Discretization is no less than 20 points per interhole spacing. For the calculation of the photonic crystals' band structure, the unit cell, as shown in the inset of Fig. 1, is chosen to facilitate finite-difference mesh generation. The computational domain can be as large as $60 \times 40 \times 400$ cells, depending on the thickness of the structure. The domain is terminated by periodic boundary conditions in the plane and by Berenger's perfectly matched layer absorbing boundary condition[3] in the vertical direction. For defect waveguide mode calculations the computational domain can be as large as $20 \times 600 \times 400$ cubic cells and is terminated by Berenger's perfectly matched layer absorbing boundary condition, except in the propagation direction, where a periodic boundary condition is applied instead. An order-N conformal technique[4] is applied in handling cylinders to overcome the staircase of the original Cartesian-grid FDTD formulation. In both cases the eigenmodes are given by the peaks in the frequency spectrum of the complex field components recorded at various low-symmetry locations[5] for a given in-plane propagation constant β.

Several defect waveguide modes are observed in the photonic bandgap. Here we deal with only the lowest-order even mode in the bandgap, which is marked with a thicker curve in the dispersion diagram. The vertical-radiation light cone and transverse radiating region of the photonic crystal are mapped as light gray and dark gray areas, respectively.

To calculate the vertical radiation loss, the photonic-crystal slab waveguide is excited by a single-frequency dipole source, the frequency of which is given by the phase shift across the unit cell used in the periodic boundary condition. A traveling field is emulated by means of double orthogonal excitation[6] in which a sinusoidal excitation is applied to the real parts of the field component and a cosinusoidal excitation is applied to the imaginary parts. The energy of unwanted modes is suppressed by applying a time domain Blackman window,[7] at least 30,000 time steps, with a side-mode suppression ratio larger than 57 dB and a bandwidth of less than 0.005 in normalized frequency. The Poynting vectors through the top and bottom planes in the vicinity of the perfectly matched layer are summed up at every instant as vertical power flow. Those through the longitudinal plane are summed as in-plane power flow. The vertical radiation loss is calculated from the ratio of the vertical power flow to the in-plane flow after a steady state is achieved. By employing the periodic boundary condition and the filter window, this model emulated an infinitely long waveguide structure and thereby eliminates the confusion incurred by mode excitation efficiency and surface-wave propagation in loss calculations if a finite-length waveguide is used. The numerical noise of the method is estimated to be less than $0.01\ \mathrm{cm}^{-1}$, which is the out-of-plane

0146-9592/03/191781-03$15.00/0

Report Documentation Page

Form Approved
OMB No. 0704-0188

1. REPORT DATE **01 JUN 2005**	2. REPORT TYPE **N/A**	3. DATES COVERED **-**
4. TITLE AND SUBTITLE **Calculated out-of-plane transmission loss for photonic-crystal slab waveguides**		5a. CONTRACT NUMBER
		5b. GRANT NUMBER
		5c. PROGRAM ELEMENT NUMBER
6. AUTHOR(S)		5d. PROJECT NUMBER
		5e. TASK NUMBER
		5f. WORK UNIT NUMBER
7. PERFORMING ORGANIZATION NAME(S) AND ADDRESS(ES) **Department of Electrical Engineering-Electrophysics, University of Southern California, Powell Hall of Engineering, 3737 Watt Way, Los Angeles, California 90089-0271**		8. PERFORMING ORGANIZATION REPORT NUMBER
9. SPONSORING/MONITORING AGENCY NAME(S) AND ADDRESS(ES)		10. SPONSOR/MONITOR'S ACRONYM(S)
		11. SPONSOR/MONITOR'S REPORT NUMBER(S)
12. DISTRIBUTION/AVAILABILITY STATEMENT **Approved for public release, distribution unlimited**		
13. SUPPLEMENTARY NOTES **See also ADM001923.**		
14. ABSTRACT		
15. SUBJECT TERMS		

16. SECURITY CLASSIFICATION OF:			17. LIMITATION OF ABSTRACT	18. NUMBER OF PAGES	19a. NAME OF RESPONSIBLE PERSON
a. REPORT **unclassified**	b. ABSTRACT **unclassified**	c. THIS PAGE **unclassified**	**UU**	**3**	

Table 1. Photonic Crystal Defect Slab Waveguides Considered in the Calculations

	Suspended Membrane		Oxidized Lower Cladding		
Waveguide Structures	Deep Undercut	Shallow Undercut	Thin Oxide	Thick Oxide	Deeply Etched
Layer description [a,b]	Air (>3.0)	Air (>3.0)	Air (>3.0)	Air (>3.0)	Air (>3.0)
					AlGaAs (1.0)
	GaAs (0.6)	GaAs (0.6)	GaAs (0.6)	GaAs (0.6)	GaAs (1.0)
	Air (3.0)	Air (1.0)	Al_xO_y (2.0)	Al_xO_y (5.0)	AlGaAs (6.0)
	GaAs substrate (>3.0)	GaAs substrate (>3.0)	GaAs substrate (>3.0)	GaAs substrate (>3.0)	GaAs substrate (>3.0)

[a]A refractive index of 3.4 is assumed for GaAs, 3.0 for AlGaAs, 1.6 for Al_xO_y, and 1.0 for air.
[b]The normalized thickness d/a appears in parentheses after the material.

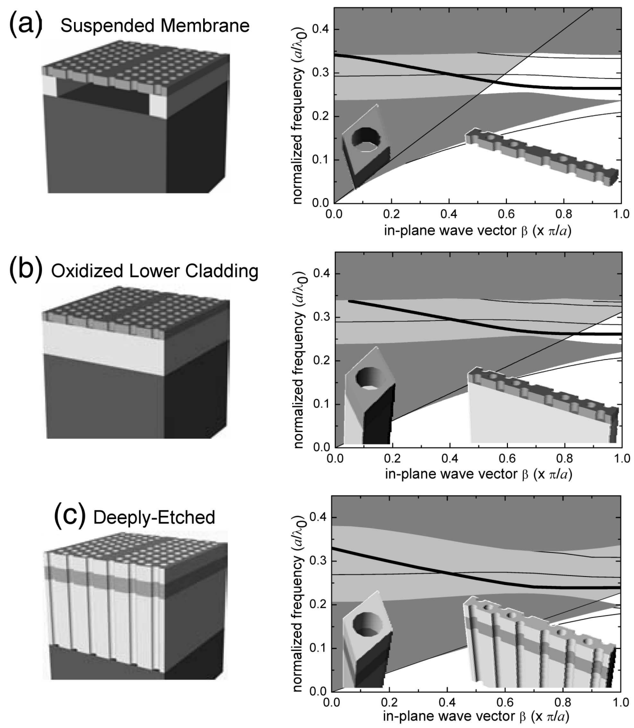

Fig. 1. Illustration of (a) suspended-membrane, (b) oxidized-lower-cladding, and (c) deeply etched structures and their dispersion diagram for vertically even (TE-like) guided modes. Inset on the dispersion diagrams are the unit cells applied in the photonic crystal and the defect waveguide band structure calculations.

radiation loss calculated by this method for a rigorously guided ridge waveguide.

The out-of-plane transmission loss as a function of the in-plane propagation constant β is plotted in Fig. 2(a). The plot covers the guided frequency range in each case. Since this loss does not include in-plane radiation loss or loss resulting from fabrication imperfection, it should be viewed as a lower limit to the loss expected for real devices. As can be seen from the plot, loss is generally high, because the Bloch mode is above the substrate light line for all cases. A thick low-index bottom cladding layer is required for isolating the guided modes from the radiation modes of the substrate. Still, radiation through the bottom cladding generally dominates the out-of-plane radiation loss. The deep undercut structure suffers the least vertical radiation loss among all the waveguides considered and has a minimum loss of approximately 0.2 cm^{-1} caused by the remaining evanescent coupling between the waveguide mode and the radiation modes of the high-index substrate. For the deep undercut structure, if the defect waveguide is designed to operate at approximately 1.55 μm with $a = 400$ nm, the membrane is suspended by 1.2 μm above the GaAs substrate. We note that the out-of-plane radiation loss of a membrane waveguide suspended by only 400 nm is 10 cm^{-1} at its minimum. This loss is 50 times that of the former structure. A similar trend holds for the oxidized-lower-cladding structures, for which a thicker oxide cladding yields lower out-of-plane radiation loss. For the deeply etched structure, the loss that is due to out-of-plane radiation is large. There exists a range of frequencies for which this loss is approximately 100 cm^{-1}, which may be acceptable for the small propagation lengths associated with integrated photonic circuitry. It should also be noted that deeply etched waveguides formed by removing multiple rows of holes have been demonstrated with significantly lower radiation loss.[8,9] Our calculations indicate that a reduction in the radiation loss by more than 3 orders of magnitude for these structures is possible. However, these waveguides are multimode at all frequencies.

The out-of-plane transmission loss as a function of normalized frequency is shown in Figs. 2(b) and 2(c). A wavelength scale is also included with $a = 420$ nm in Fig. 2(b) and 450 nm in Fig. 2(c). The plots break off abruptly at the lower end of the frequency range because of the cutoff frequency of the guided mode considered in this Letter. The vertical radiation loss for frequencies lower than the cutoff frequency is not a property of the guided mode and therefore is not the subject of this discussion.

The bandwidth of low-loss (<1-cm^{-1}) operation for suspended-membrane defect waveguides is approximately 60 nm when operating around 1550 nm as the central working wavelength. For oxidized-lower-cladding defect waveguides the range of wave vectors under the cladding light line is reduced as a result of the higher refractive index compared with that in the suspended-membrane case. That range, which is in the vicinity of the Brillouin-zone boundary, also corresponds to the low-group-velocity region.

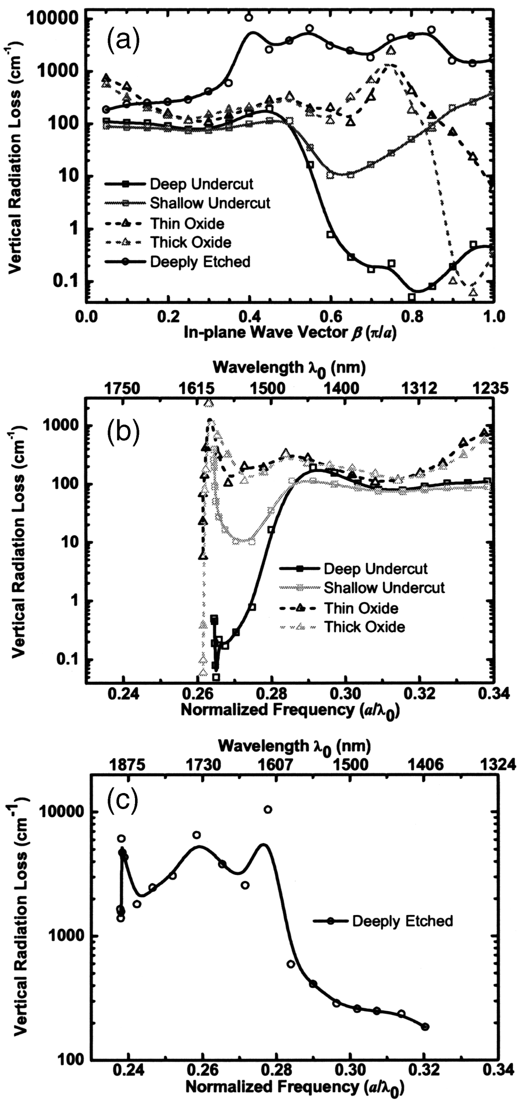

Fig. 2. Out-of-plane radiation loss as a function of (a) the in-plane wave vector β and (b), (c) the normalized frequency for the photonic-crystal defect slab waveguides modeled in this work. The lattice constant $a = 450$ nm for the deeply etched waveguide and 420 nm for the rest of the cases. Points are calculated values, and curves are B-spline curve fits.

Consequently, oxidized-lower-cladding structures allow a much narrower bandwidth, less than 3 nm near 1550 nm in this case. However, by tuning the waveguide structure by means of the defect width,[10–12] hole radius,[10] and hole shape, a broader bandwidth for an oxidized-lower-cladding or sapphire-clad defect waveguide can be obtained.

In summary, a numerical model was developed to analyze the out-of-plane propagation loss of linear defect photonic-crystal slab waveguides. The results show that, for a sufficiently thick bottom cladding layer, both the suspended-membrane and oxidized-lower-cladding structures are capable of low-loss transmission over a limited range of frequencies.

This research was supported by the National Science Foundation under grant ECS 0094020. Computation for the work was, in part, supported by the University of Southern California Center for High Performance Computing and Communications. W. Kuang's e-mail address is wkuang@usc.edu.

References

1. K. S. Yee, IEEE Trans. Antennas Propag. **AP-14,** 302 (1966).
2. A. Taflove, *Computational Electrodynamics: The Finite-Difference Time-Domain Method* (Artech House, Norwood, Mass., 1995).
3. J.-P. Berenger, J. Comput. Phys. **127,** 363 (1996).
4. C. T. Chan, Q. L. Yu, and K. M. Ho, Phys. Rev. B **51,** 16635 (1995).
5. D. H. Choi and W. J. R. Hoefer, IEEE Trans. Microwave Theory Tech. **34,** 1464 (1986).
6. M. Celuch-Marcysiak and W. K. Gwarek, IEEE Trans. Microwave Theory Tech. **43,** 860 (1995).
7. A. V. Oppenheim and R. W. Schafer, *Discrete-Time Signal Processing* (Prentice-Hall, Englewood Cliffs, N.J., 1989).
8. A. Talneau, L. Le Gouezigou, and N. Bouadma, Opt. Lett. **26,** 1259 (2001).
9. C. J. M. Smith, Appl. Phys. Lett. **77,** 2813 (2000).
10. M. Loncar, J. Vuckovic, and A. Scherer, J. Opt. Soc. Am. B **18,** 1362 (2001).
11. M. Notomi, A. Shinya, K. Yamada, J. Takahashi, C. Takahashi, and I. Yokohama, Electron. Lett. **37,** 293 (2001).
12. W. Tung and S. Fan, Appl. Phys. Lett. **81,** 3915 (2002).